Supplemental Information for:

Selection through soft and incomplete sweeps underlies postglacial ecotype differentiation in an Arctic wide-ranging ungulate

Table of content

Supplementary Methods 1 : Demographic inference	2
Supplementary Methods 2 : Estimation of differentiation and diversity metrics	3
Supplementary Methods 3 : Imputation of low-coverage data and validation	3
Supplementary Methods 4 : Comparison of diversity metrics in peaks	4
Schematic overview of bioinformatic methods	5
References	6
Supplementary Table legends	7
Supplementary Figure	
S1	8
S2	8
S3	9
S4	10
S5	11
S6	12
S7	13
S8	14

Supplementary Methods

1. Demographic inference

We built four alternative two-population demographic models of increasing complexity: 1) strict isolation (SI, 4 parameters), where the ecotypes diverged at time t_d from an ancestral population with no subsequent gene flow; 2) isolation with migration (IM), adding asymmetrical gene flow after divergence; 3) second contact (SC), where a period in isolation is followed by gene flow between ecotype after time t_m; and 4) ancient migration (AM), similar in complexity to SC, with gene flow following divergence that stopped at time t_m.

For each demographic model, we performed 100 independent parameter optimization runs, each consisting of 40 expectation–conditional maximization (ECM) cycles (-L) and 200,000 coalescent simulations (-n) per likelihood estimation. Migration rate was set to 3.47×10^{-8} mutations/site/generation, as estimated in Dedato et al. (2022). Cells of the SFS with fewer than 10 SNPs (-C) were ignored. Parameter values were drawn from log-uniform prior distributions, with effective population sizes bounded between 100 and 1,000,000 individuals; migration rates between 10^{-6} and 10^{-2} migrants/generation; t_d between 100 and 10,000 generations; and t_m between 0.1 and $0.9 \times t_d$ (uniform prior distribution). We modelled migratory-to-boreal and boreal-to-migratory gene flow independently, allowing for asymmetry. For each model, the run with the highest likelihood across replicates was retained. Model support was then compared using the Akaike Information Criterion (AIC).

For best supported models, we checked if adding growth parameters after divergence improve the fit of the model. We optimized three new models (growth in migratory, in boreal, or in both) in the same way as before, while exploring growth rate bounded between -5×10^{-4} and 5×10^{-4} (uniform distribution of priors) to allow for either growth or decline of N_e. We then compared the AIC from the run with the highest likelihood to the corresponding model without growth.

To estimate confidence intervals around demographic parameters, we performed parametric bootstrapping under the best-supported models, following Excoffier et al. (2021). Specifically, we generated 100 pseudo-observed site frequency spectra (SFS) using parameter estimates from the maximum-likelihood run. Each simulated dataset was then reanalyzed over 30 runs using the same inference procedure and optimization settings as for the empirical data. Confidence intervals (95%) for each parameter were obtained from the empirical distribution of

parameter estimates across bootstrap replicates, using the 2.5th and 97.5th percentiles.

2. Estimation of differentiation and diversity metrics

We first used realsfs fst index, print, stats and stats2 functions in ANGSD and the genome-wide 2D-SFS as prior to estimate windowed weighted F_{ST} (Reynolds et al., 1983). To insure local F_{ST} was not inflated due to imbalanced sampling design or genomic features with reduced recombination such as pericentromeric regions or large structural variants, we permuted individuals to create two biologically irrelevant groups on which we recomputed windowed F_{ST}. We repeated this procedure ten times to create a null distribution of F_{ST} for each window, then subtracted the average permuted F_{ST} across runs to our F_{ST} between ecotypes. This value is hereafter reported as bootstrapped F_{ST} (bF_{ST}), following Merondun et al. (2025). Windows with the bF_{ST} in the top 0.2% across autosomes were defined as peaks of differentiation and considered as candidate regions for divergent selection between ecotypes.

We also estimated windowed d_{xy} by repeating SAF computation and 2D-SFS estimation in each window, using the same procedure and parameters as chromosome-wide SFS. We then used the dxy_wsfs.py script (Marques et al., 2018) that we modified to extract the number of sites that passed coverage filters per window. Finally, we built 1d-SFS per ecotype to estimate Watterson's estimator (θ_W), nucleotide diversity (θ_π) and Tajima's D in windows through the realsfs saf2theta and do_stat functions.

We repeated the estimation of bF_{ST}, d_{xy}, θ_W, θ_π, and Tajima's D on the X chromosome while considering only unrelated females (n = 20 migratory and 29 boreal), then defined peaks of differentiation as the windows top 0.2% bF_{ST} on the X chromosome. We ignored windows for which more than half (25kb) the sites had insufficient coverage (less than 90% of samples with ≥ 1X) or were masked from the reference following paralog detection.

3. Imputation of low-coverage data and validation

To impute our low-coverage dataset, we build a reference panel using the high-coverage data, as it contained representatives of all subpopulations studied here. We used bcftools v1.22 (Danecek et al., 2021) mpileup and call on the combined low-coverage and high-coverage bam files, in order to include a maximum of polymorphic sites in the vcf, then kept only genotypes from high-coverage samples for further filtration and phasing. Biallelic variants on autosomes were retained if they passed standard filtering thresholds including a minimum variant quality score (QUAL ≥ 30),

mapping quality (MQ ≥ 30), site depth between 200 and 2000, low variant distance bias (VDB > 1×10^{-6}), and a low proportion of reads with zero mapping quality (MQ0F < 0.1). We excluded SNPs within 75bp of a putative paralog (see ngsParalog above) to avoid spurious genotypes biasing our phasing. SNPs with more that 10% of missing data were removed, then remaining missing data were imputed as the most frequent homozygote. We used Whatshap 2.3 (Martin et al., 2023) to phase the reference vcf using the high-coverage bam files as input. We then used Glimpse 2.0.1 (Rubinacci et al., 2021) to split autosomes in chunks to be phased and imputed using the genotype-likelihood low-coverage bcf as input (--input-gl) and the phased high-coverage vcf as reference. We then ligated chunks by chromosomes and used bcftools to filter the newly imputed vcf to remove sites with MAF < 0.05 and an INFO score under 0.8. We repeated the same process for the reference and imputation on chrX while using only data from confirmed females.

To validate the accuracy of imputation, we used samtools view -s to subsample a fraction of reads in the bam files from the high-coverage samples, aiming for a genome-wide coverage equals to the average coverage in the low-coverage data, as estimated with mosdepth earlier. We ran our ANGSD pipeline a second time as described above on the low-coverage and subsample samples, then imputed the genotypes in GLIMPSE. We then used bcftools isec to intersect the SNPs called in the high-coverage reference (MAF > 0.01 among the high-coverage samples) and those imputed from the subsampled dataset. For each high-coverage sample, we calculated the proportion of identical genotypes between the called and imputed data and reported those proportions by sample and bins of allelic frequency in the called genotypes.

4. Comparison of diversity metrics in peaks

To compare θ statistics, Tajima's D, dxy, and XP-nSL in peaks of differentiation and the genomic background, we used block bootstrapping of the genome to generate a null distribution that preserves the spatial autocorrelation of genomic variation across chromosomes. Specifically, we repeatedly sampled genomic blocks matching the observed distribution of peak sizes (merged merging overlapping windows with the top 0.2% bF_{ST}) and computed the mean and standard deviation of diversity metrics for each replicate, allowing us to obtain an empirical expectation of both the mean and variance under genome-wide structure. From these resampled distributions, we further quantified the effect size of the difference between peaks and the genomic background using Cliff's delta, which measures the probability that a randomly chosen peak region has lower diversity than a randomly chosen genomic region

(Meissel & Yao, 2024). We then derived a 95% confidence interval for Cliff's delta from the bootstrap distribution. We repeated this process to compare regions with the top 0.2% absolute normalized XP-nSL with the rest of the genome.

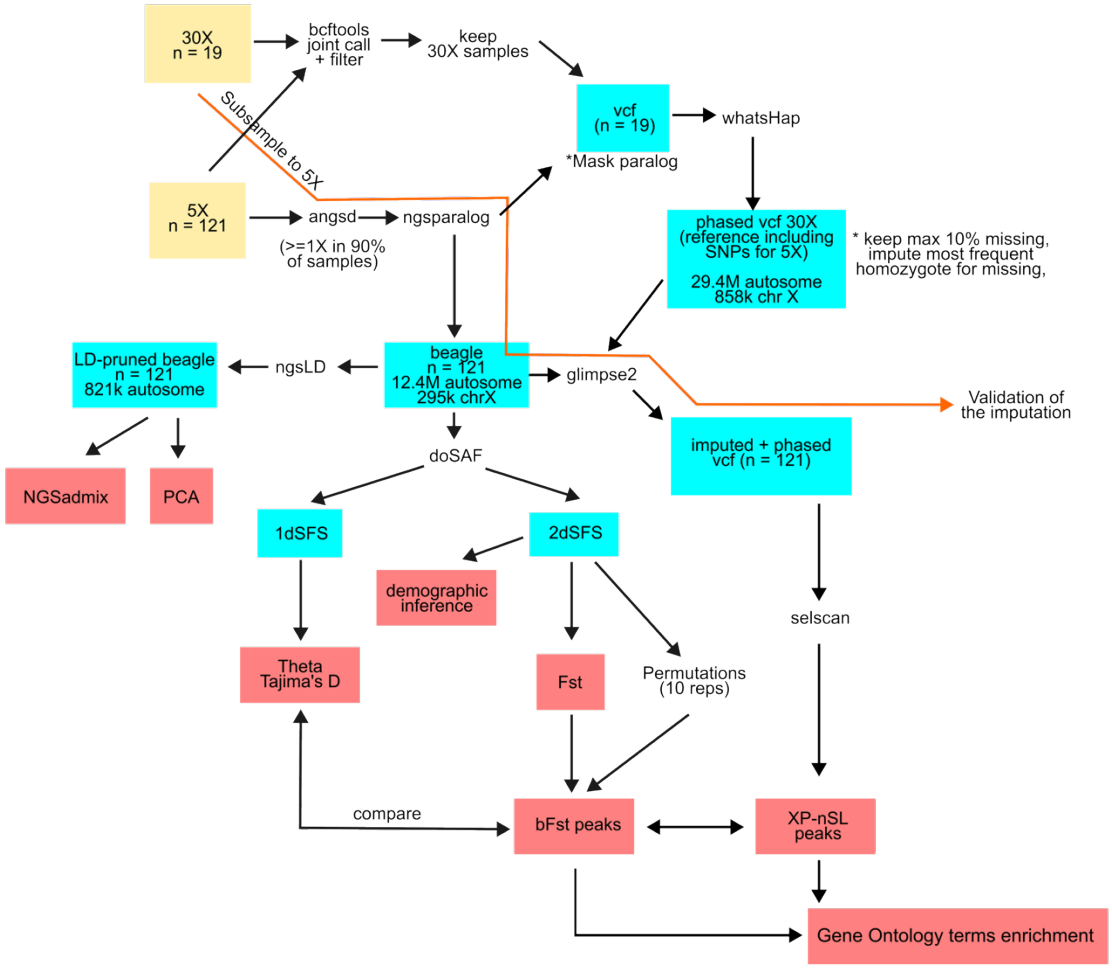

Schematic overview of bioinformatic methods

References

Danecek, P., Bonfield, J. K., Liddle, J., Marshall, J., Ohan, V., Pollard, M. O., Whitwham, A., Keane, T., McCarthy, S. A., Davies, R. M., & Li, H. (2021). Twelve years of SAMtools and BCFtools. *GigaScience*, *10*(2). https://doi.org/10.1093/gigascience/giab008

Dedato, M. N., Robert, C., Taillon, J., Shafer, A. B. A., & Côté, S. D. (2022). Demographic history and conservation genomics of caribou (Rangifer tarandus) in Québec. *Evolutionary Applications*, *15*(12), 2043–2053. https://doi.org/10.1111/eva.13495

Excoffier, L., Marchi, N., Marques, D. A., Matthey-Doret, R., Gouy, A., & Sousa, V. C. (2021). *fastsimcoal2* : demographic inference under complex evolutionary scenarios. *Bioinformatics*, *37*(24), 4882–4885. https://doi.org/10.1093/bioinformatics/btab468

Marques, D. A., Jones, F. C., Di Palma, F., Kingsley, D. M., & Reimchen, T. E. (2018). Experimental evidence for rapid genomic adaptation to a new niche in an adaptive radiation. *Nature Ecology & Evolution*, *2*(7), 1128–1138. https://doi.org/10.1038/s41559-018-0581-8

Martin, M., Ebert, P., & Marschall, T. (2023). Read-Based Phasing and Analysis of Phased Variants with WhatsHap. In B. A. Peters & R. Drmanac (Eds.), *Haplotyping* (Vol. 2590, pp. 127–138). Springer US. https://doi.org/10.1007/978-1-0716-2819-5_8

Meissel, K., & Yao, E. (2024). Using Cliff's Delta as a Non-Parametric Effect Size Measure: An Accessible Web App and R Tutorial. *Practical Assessment*, *Research*, Evaluation Volume 29 Issue 1 2024. https://doi.org/10.7275/PARE.1977

Merondun, J., Fossøy, F., Meshcheryagina, S., Atkinson, P., Bachurin, G., Bulyuk, V., Fenchuk, V., Golovatin, M., Hewson, C., Honza, M., Markovets, M., Moskát, C., Owens, G. L., Procházka, P., Red'kin, Y., Rutila, J., Thorup, K., Stokke, B. G., Liang, W., & Wolf, J. B. W. (2025). Genomic architecture of egg mimicry and its consequences for speciation in parasitic cuckoos. *Evolution*, *390*(6772), 527–532. https://doi.org/10.1126/science.adt9355

Reynolds, J., Weir, B. S., & Cockerham, C. C. (1983). Estimation of the Coancestry Coefficient: Basis for a Short-Term Genetic Distance. *Genetics*, *105*(3), 767–779. https://doi.org/10.1093/genetics/105.3.767

Rubinacci, S., Ribeiro, D. M., Hofmeister, R. J., & Delaneau, O. (2021). Efficient phasing and imputation of low-coverage sequencing data using large reference panels. *Nature Genetics*, *53*(1), 120–126. https://doi.org/10.1038/s41588-020-00756-0

Supplementary tables

Table S1: Summary of sample size and number of filtered SNPs in the low and high coverage datasets at various stages of the analysis.

Table S2: Potentially adaptive CNV in the migratory and boreal ecotypes as identified in Prunier et al. (2022) and their position on the Svalbard reindeer assembly.

Table S3: Comparison of diversity, differentiation and haplotype-based metrics between peaks of bFST or |XP-nSL| (and their overlap) and the genomic background on autosomes. Size of effect was assessed using Cliff's δ after block bootstrapping.

Table S4: Genes inferred through homology that overlapping peaks of bFST or |XP-nSL| (and their overlap).

Table S5: Enriched gene functions (biological processes) for genes overlapping peaks of bF_{ST} or |XP-nSL| (and their overlap). Peaks of |XP-nSL| were further divided between the ecotypes in which positive selection was inferred based on the sign of XP-nSL.

Supplementary figures

Figure S1: Confirmation of genetic sex in the high and low-coverage dataset, through relative depth of coverage on sex chromosome (depthX, depthY) and depth of autosomes (depthA). Sex assigned at capture is denoted in color.

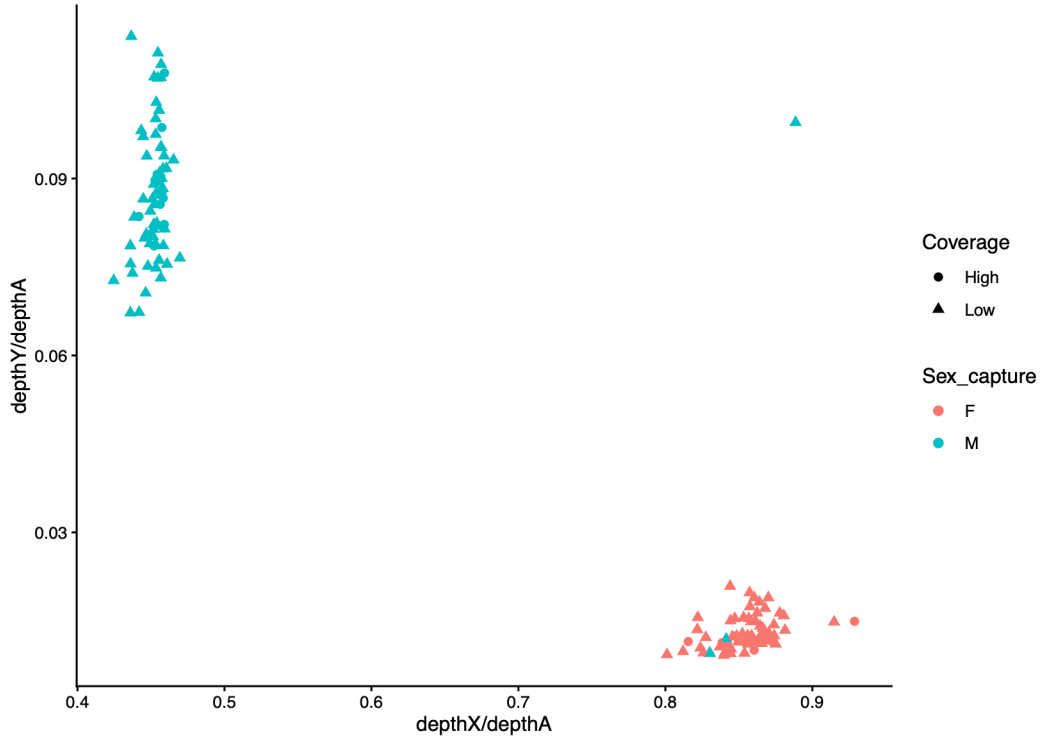

Figure S2: Genome-wide average depth of coverage in the low (left) and high (right) coverage datasets

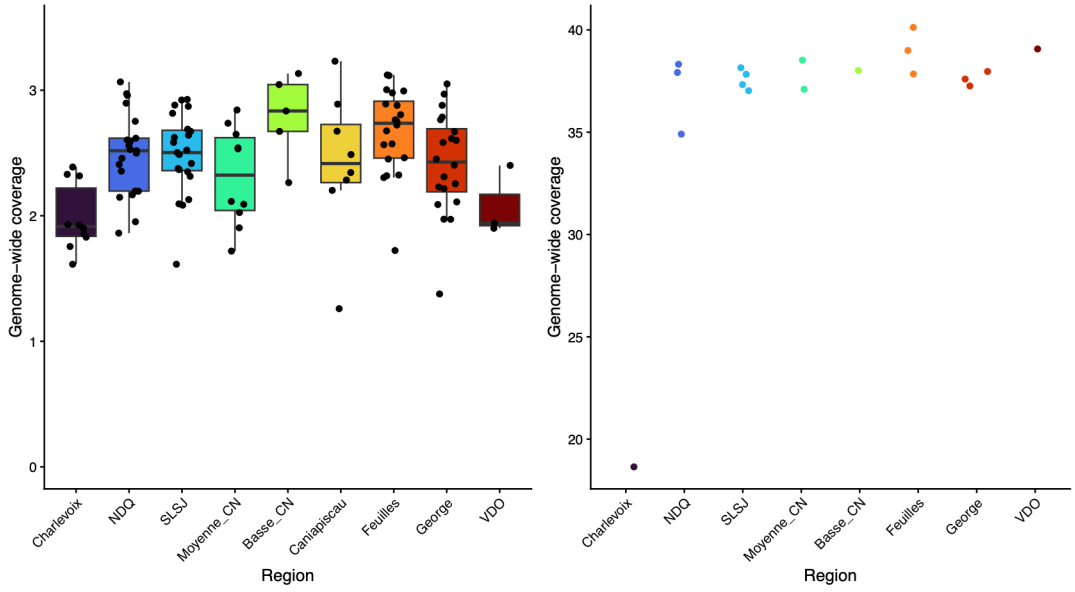

Figure S3: Akaike Information Criterion (AIC) for 100 runs of the isolation with migration (IM, left) and the secondary contact (SC, right) models with various growth parameters added. The first letter specifies growth/decline (G) in the migratory population or constant size (g), whereas the second G/g indicates growth/decline or the lack of in the boreal population.

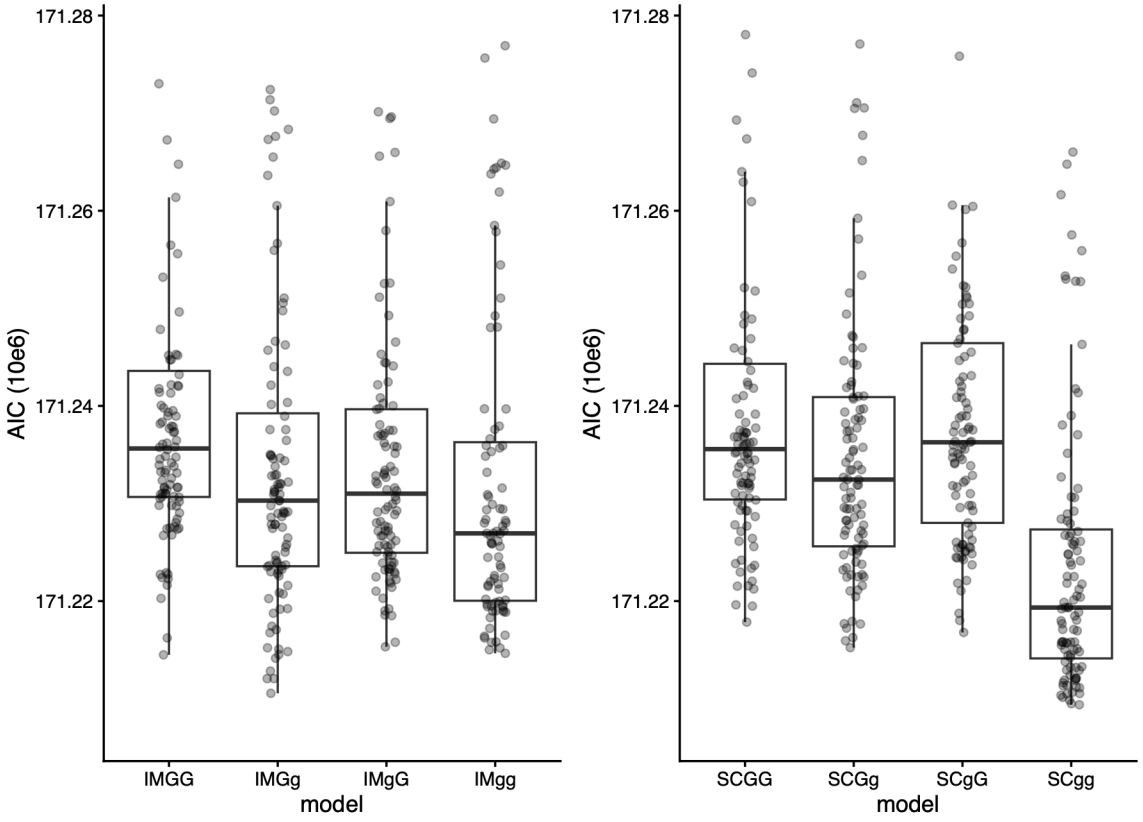

Figure S4: Comparison of concordance for samples in the high-coverage datasets, between their called and imputed (after random subsampling of reads to ~3X) genotypes. Allele frequency classes are delimited by dashed vertical lines and individual samples are connected across classes by a line with color matching their ecotype

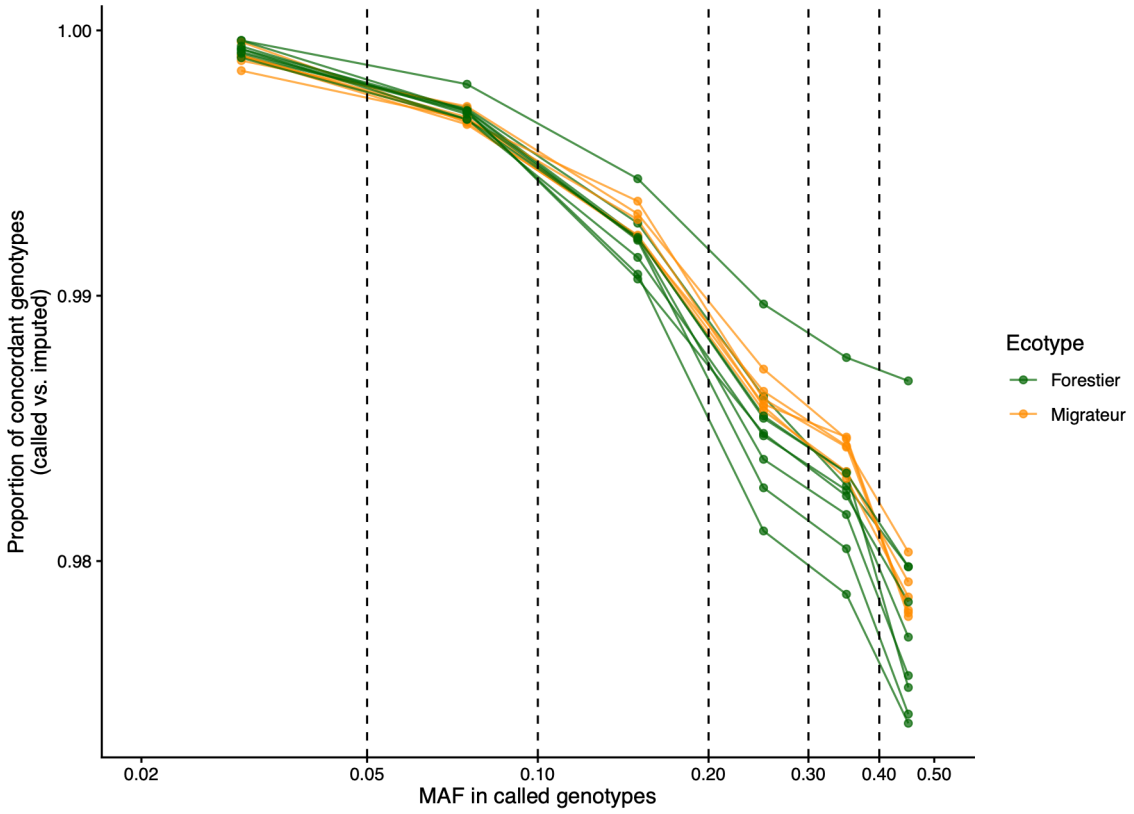

Figure S5: Density plots for differentiation, diversity and haplotype metrics, with top 0.2% and 1% thresholds

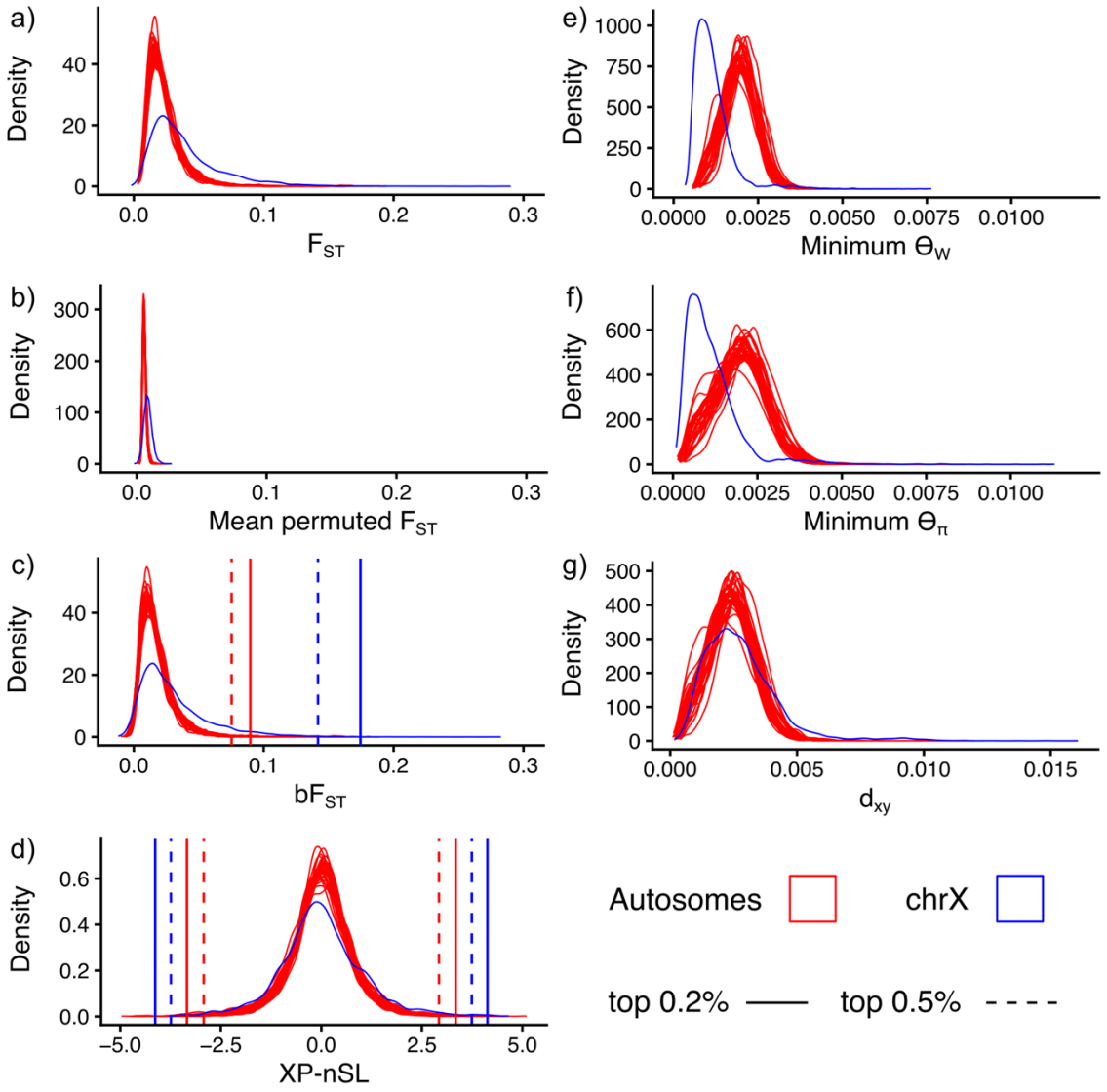

Figure S6: Correlation between metrics in 50kb overlapping windows on autosomes. Number of sites (nSites), number of SNPs (nSNPs), F_{ST} and bootstrapped F_{ST} (bfst), |XP-SNL| (abs.xpnsl), θ_W (mintW) and θ_π (mintP) for the ecotype witht the lowest value, and d_{xy} were compared.

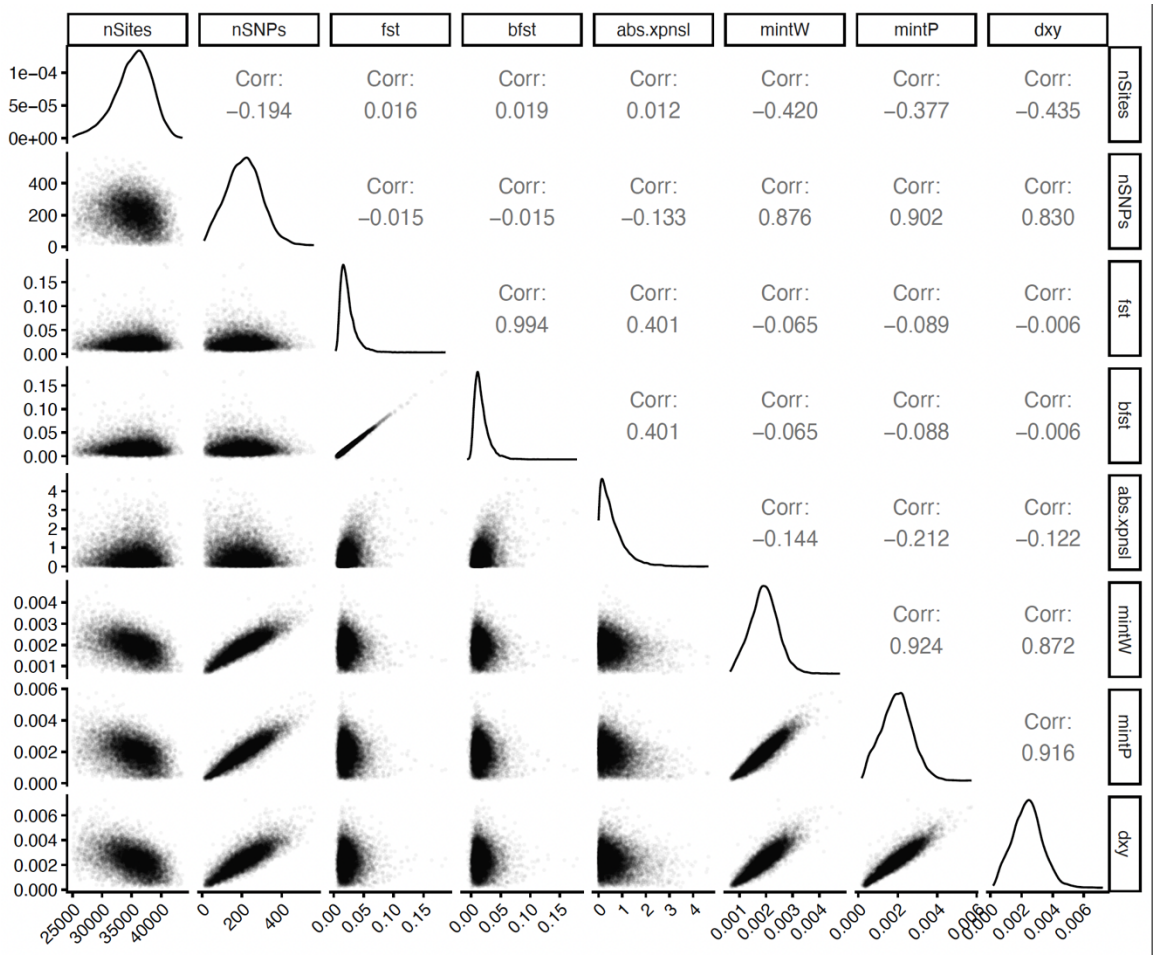

Figure S7: Comparison of XP-nSL, d_{xy}, θ metrics, and Tajima's D in peaks of bFst (blue) and the genomic background (red). XP-nSL was further divided between windows where XP-nSL > 0 (orange) and XP-nSL < 0 (green).

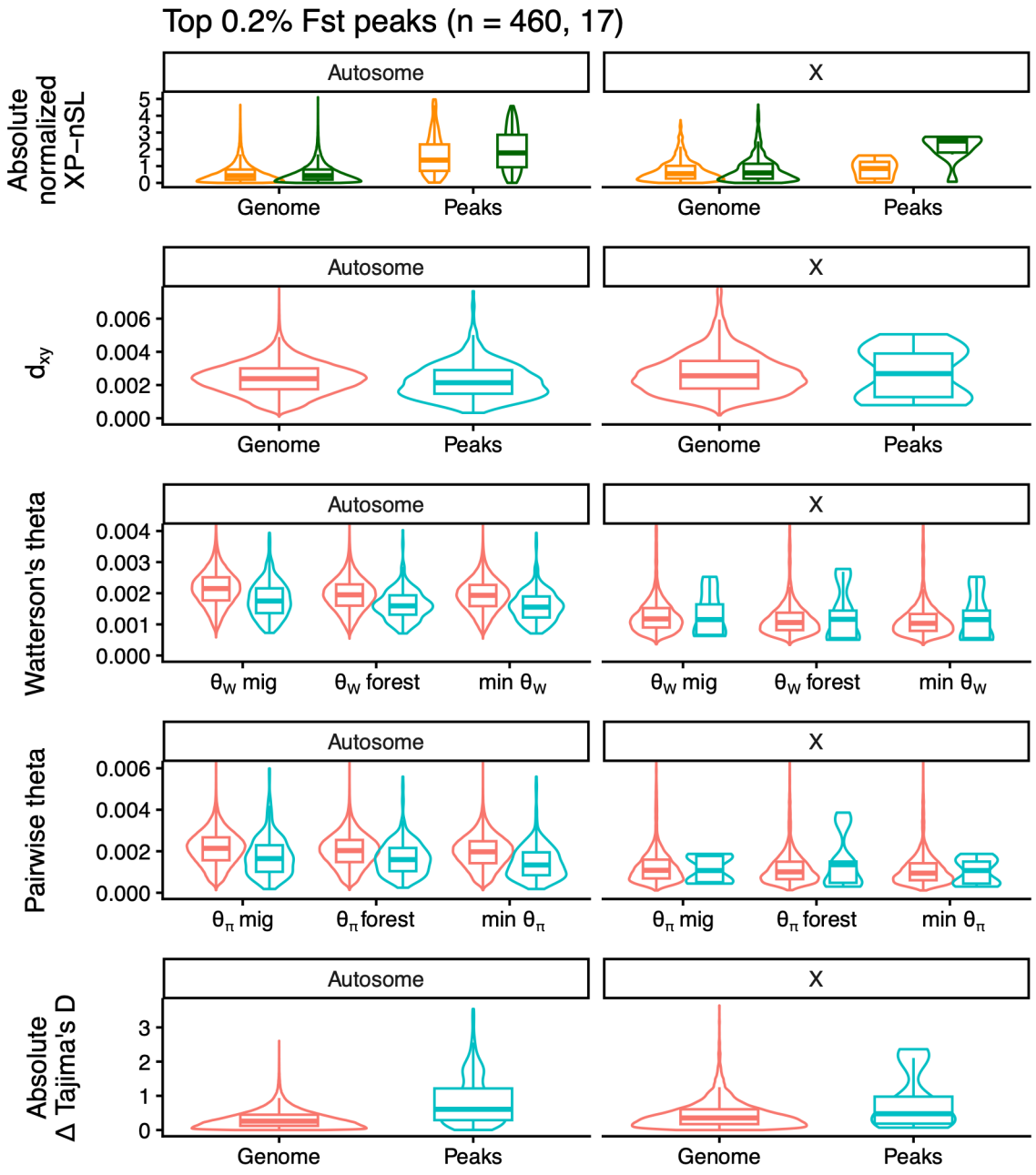
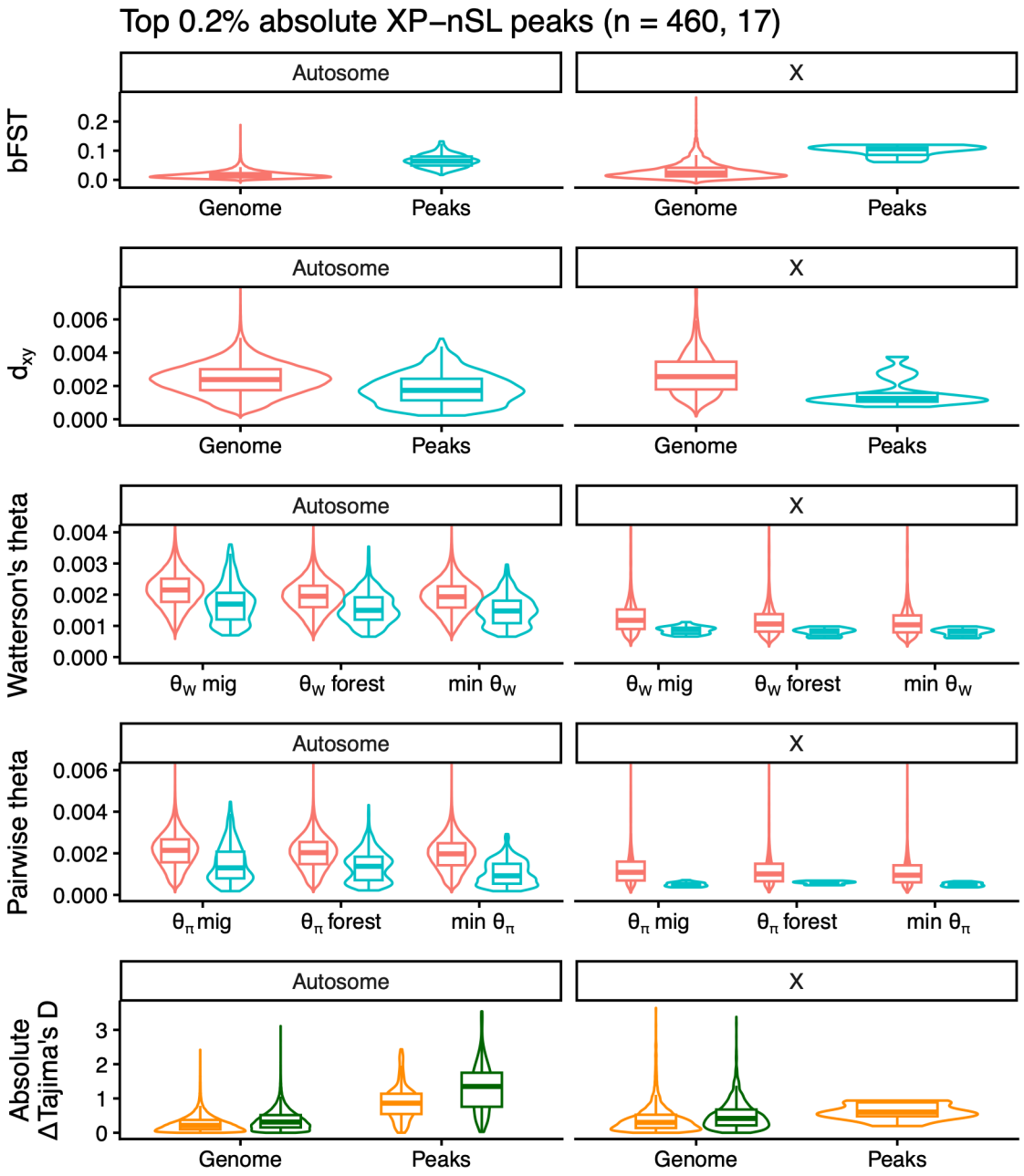
Figure S8: Comparison of bF_{ST}, d_{xy}, θ metrics, and Tajima's D in peaks of |XP-nSL| (blue) and the genomic background (red). Tajima's D was further divided between windows where XP-nSL > 0 (orange) and XP-nSL < 0 (green).